EVOLUTION

Infrared radiation is an ancient pollination signal

Wendy A. Valencia-Montoya[1,2]*, Marjorie A. Liénard[3], Neil Rosser[4], Michael Calonje[5], Shayla Salzman[6], Cheng-Chia Tsai[7], Nanfang Yu[7], John R. Carlson[8], Rodrigo Cogni[9], Naomi E. Pierce[1]*† Nicholas W. Bellono[2]*†

Color and scent are well-known pollinator cues. Some plants also produce heat, but its role remains unclear. Here, we report that plant-generated thermal infrared radiation serves as a pollination signal and describe the underlying mechanisms of heat production and infrared detection. Mitochondrial adaptations heat plant reproductive structures in a circadian pattern, radiating infrared that is sufficient to attract beetle pollinators. Beetle antennae contain infrared-activated neurons with thermosensitive ion channels that are structurally tuned to match host plant thermogenesis. Comparative analyses revealed that infrared is among the earliest pollination signals, and indicate a deep-time transition from infrared-based to color-dominated signaling in flowering plants. Our findings uncover an ancient sensory modality shaping the early evolution of pollination, one of the world's most vital processes linking plants and animals.

Plants have evolved an astonishing repertoire of cues to attract pollinators. Although color, scent, and humidity are well-appreciated pollination signals (*1*–*3*), some plants also produce heat (*4*). Similar to endothermic animals, thermogenic plants generate heat as a by-product of cellular respiration (*5*). Thermogenic plants can achieve cellular respiration rates comparable to that of a "hummingbird in flight", leading to an increase in temperature to more than 35°C above ambient temperature (*4*, *6*). Plant thermogenesis has been linked to preventing frost tolerance (*7*), enhancing scent volatilization (*5*, *8*), and providing a warm shelter for pollinators (*9*). However, it may also function as a direct cue (*10*), because thermogenesis occurs exclusively in reproductive organs such as cones (gymnosperms) and flowers (angiosperms), with immense variation in thermal patterns reminiscent of other pollination signals such as color.

Heat produced by flowers and cones can spread through conduction, convection, or infrared radiation (IR). Unlike conduction and convection, IR could represent an effective signal for pollinators because it emanates in all directions and does not require contact. Thermal IR is a sensory cue used by many animals to locate the warm bodies of prey. Snakes, vampire bats, blood-sucking mosquitoes, fire beetles, and flat bugs use IR to localize their endothermic prey, hosts, or forest fires. Considering that most thermogenic plants begin to heat at dusk and are pollinated at night, when IR is especially conspicuous (*5*, *11*), we investigated whether pollinators could use IR as a foraging signal.

Cycads are the oldest living lineage of seed plants pollinated by animals and collectively account for more than half of all known thermogenic plant species (*12*–*16*). These gymnosperms have distinct male and female reproductive organs that are produced on separate plants and engage in daily cycles of volatile emissions that trigger beetle pollinator movement between male (pollen) and female (ovulate) cones (*12*). Extensive fossil evidence suggests that cycad interactions with beetle pollinators are highly specialized and date back at least to the early Jurassic, around 200 million years ago (Ma) (*17*). We therefore focused on cycads and beetles as a model system to investigate the role of thermal IR in plant-pollinator signaling and the early evolution of pollination mutualisms.

Molecular basis of thermogenesis in cycads

We first took thermal images of the cycad *Zamia furfuracea* to confirm that heat production occurs primarily in the sporophylls of pollen-shedding cones (Fig. 1, A to C). Plant thermogenesis is controlled by mitochondrial respiration. During this process, carbohydrates or lipids fuel heat production through alternative oxidase (AOX) or uncoupling proteins, which bypass adenosine 5′-triphosphate (ATP) synthesis to dissipate redox energy as heat (*13*, *18*–*20*). Accordingly, we found that sporophylls from the cycad *Z. furfuracea* contained more mitochondria compared with nonthermogenic tissues and up-regulated *AOX1* just before and during thermogenesis (Fig. 1, D and E, and fig. S1, D to H). We also observed up-regulation of genes related to carbohydrate transport and starch metabolism, as well as numerous starch-filled amyloplasts in sporophyll tissues that were depleted after thermogenesis (Fig. 1, D and E; fig. S2; and tables S1 and S2). These results highlight *AOX1* as a major regulator for respiration across cycads that uses starch as the primary substrate for thermogenesis.

We also found that cones up-regulated circadian clock genes during thermogenesis, including *REVEILLE* (*RVE*) transcription factors, which are involved in afternoon and early evening rhythms (Fig. 1E) (*21*). Indeed, measuring thermogenic activity over time uncovered a strong circadian pattern with a single daily burst of heat production starting in the afternoon and peaking in the early evening (Fig. 1F). We then extended our sampling of thermogenic patterns across the major lineages of the genus *Zamia*, the largest neotropical radiation of cycads, to find that all sampled species were thermogenic and under circadian control (Fig. 1, G and H, and table S3). Thus, thermogenesis in *Zamia* is conserved, energetically expensive, tightly time regulated, and only observed in plant organs involved in pollination (Fig. 1, B and C).

IR is a pollination signal

Cycads are dioecious, with separate male and female plants. We found that in all sampled *Zamia* species, pollen (male) and ovulate (female) plants exhibited distinct circadian dynamics (Fig. 2, A to D, and fig. S3, A to C). Male cones of *Z. furfuracea* heated first and then cooled, whereas female cones entered peak thermogenesis ~3 hours later (Fig. 2D and fig. S3C). This observation led us to investigate the relationship between plant thermogenesis and pollinator behavior. We tracked the movement of *Rhopalotria furfuracea*, the beetle pollinator of *Z. furfuracea*, in an open-field experiment in which female and male plants were placed 50 m apart. By marking beetles with ultraviolet (UV)–fluorescent dyes to track their visits, we discovered that beetles were preferentially drawn to the warmest regions of pollen cones, suggesting that cone thermal patterns might serve as pollination guides (Fig. 2C and figs. S3D and S4). Next, we monitored beetle movement in controlled cages and found that occupancy of male and female cones correlated with the rise and fall of sex-specific cone temperature (Fig. 2D). In fact, we hypothesized that decreases in cone temperature could act as a dynamic signal for the beetles to leave the pollen cones and visit the ovulate cones (Fig. 2D). These experiments demonstrated that beetles actively move between male and female cones during thermogenic events.

In cycads, this "push-pull" pollination mechanism was thought to be primarily driven by the emission of species-specific cone volatiles

[1]Department of Organismic and Evolutionary Biology and Museum of Comparative Zoology, Harvard University, Cambridge, MA, USA. [2]Department of Molecular and Cellular Biology, Harvard University, Cambridge, MA, USA. [3]GIGA Institute, Liège University, Liège, Belgium. [4]Department of Biology, University of Miami, Coral Gables, FL, USA. [5]Montgomery Botanical Center, Coral Gables, FL, USA. [6]Department of Entomology, University of Georgia, Athens, GA, USA. [7]Department of Applied Physics and Applied Mathematics, Columbia University, New York, NY, USA. [8]Department of Molecular, Cellular & Developmental Biology, Yale University, New Haven, CT, USA. [9]Departamento de Ecologia, Universidade de São Paulo, São Paulo, Brazil. ***Corresponding author. Email: wvalenciamontoya@g.harvard.edu (W.V.-M.); npierce@oeb.harvard.edu (N.E.P.); nbellono@harvard.edu (N.W.B.)** †These authors jointly supervised this work.

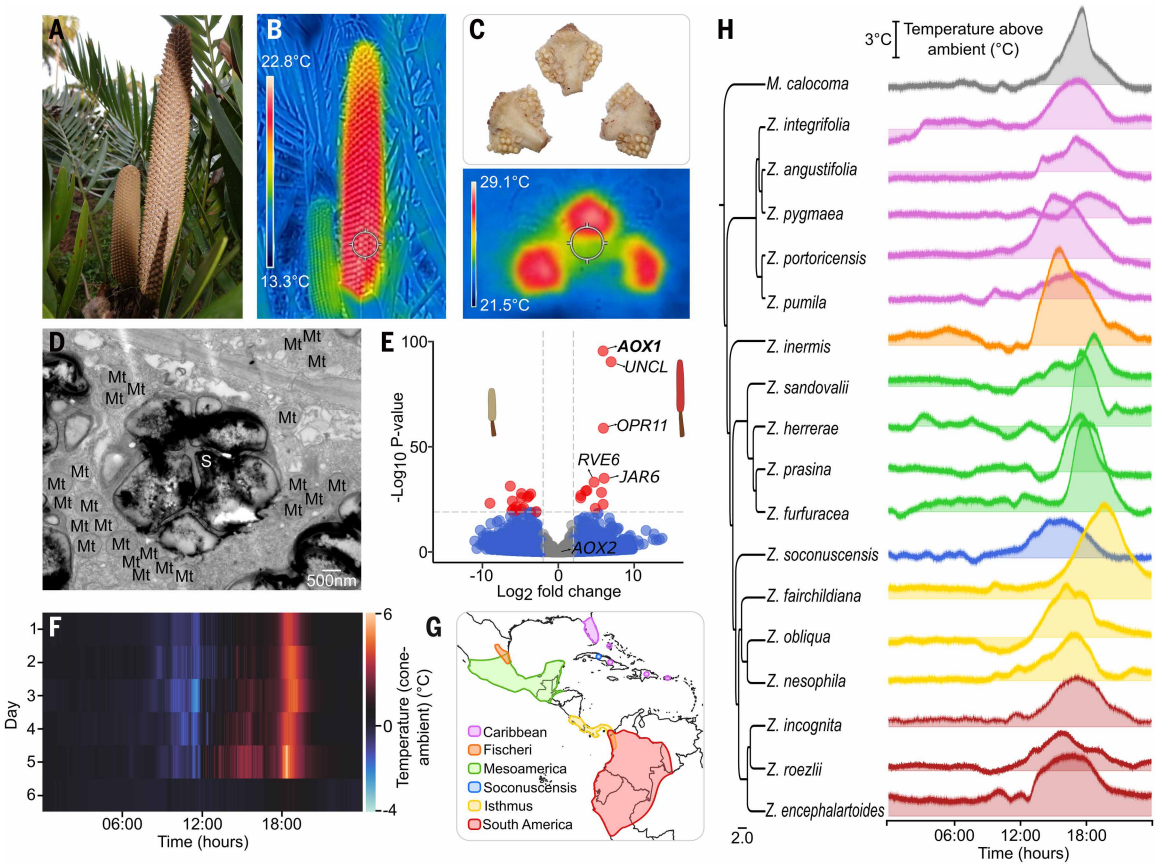

Fig. 1. Thermogenic plants have mitochondrial adaptations to heat their reproductive structures during pollination. (**A**) An open cone of a cycad plant. Cones are the reproductive structures of cycads. (**B**) Thermal infrared image of a cycad male cone heating during pollen release. (**C**) Sporophylls of the cycad *Z. furfuracea* are the primary thermogenic organs. (**D**) Transmission electron micrograph section of a cone sporophyll depicts the densely populated mitochondria (Mt) and starch granules (s) in thermogenic tissues. (**E**) Differential gene expression analysis between nonthermogenic (left) and thermogenic (right) cones. Blue points indicate transcripts with at least a twofold change in expression ($|\log_2 FC| > 2$); red points indicate transcripts meeting this threshold and also showing statistical significance ($-\log_{10} P > 20$). $n = 6$ sporophylls per condition. (**F**) Temperature above or below ambient of a cycad cone releasing pollen over several days. (**G**) Map showing the distribution of all major lineages of *Zamia*, the most diverse genus of neotropical cycads. (**H**) Cone temperature above ambient for 17 different *Zamia* species across all major clades of the *Zamia* radiation "(89 described species) and for the outgroup *Microcycas calocoma*. Colors are the same as for the distributions of *Zamia* clades in (G).

(*12*, *22*). However, the volatiles themselves and other signals, including humidity, can also correlate with plant thermogenesis (*2*, *22*). To tease apart the contribution of heat among these multiple pollination signals, we scanned cycad cones and conducted experiments with artificially heated three-dimensional (3D) models (Fig. 2, E and F). We placed model cones near real cycad plants bearing female or male cones and heated them to match either the average temperature of *Z. furfuracea* cones during thermogenesis or the ambient temperature (Fig. 2, E and F, and fig. S3G). To prevent thermal conduction, models were coated with odorless tangle trap so that beetles would be stuck to cones upon visiting and could not use touch to discern temperature differences between the 3D models; this ensured that temperature was the only variable differing between 3D cones. We found that wild beetle pollinators were more attracted to heated female and male cone models compared with ambient temperature controls (Fig. 2G).

These results suggest that emanating thermal signals such as IR could act as a short- to midrange pollination cue. To further control for convective heat transfer, we devised an enclosure experiment to transmit only thermal IR by covering the heated 3D cones with a polyethylene film (~99% transparent to IR) positioned ~1 cm from the cone surface. In this controlled environment, pollinators preferentially landed on heated female and male cones emitting higher IR, confirming that IR is a pollination signal (Fig. 2H).

Beetle pollinators use specialized antennae to sense IR

We next reasoned that if cycads and their beetle pollinators have evolved a species-specific communication channel, then beetles should also have sensory adaptations for detecting thermal IR. In insects, sensilla are the basic unit of sensory reception, and their morphology and distribution correlate with function (*23*). Most thermosensitive neurons in insects are housed in peg-in-pit coeloconic sensilla, which are small cuticular pits containing sensory pegs (*24*). Therefore, we surveyed coeloconic sensilla in two beetle species, *R. furfuracea* and *Pharaxonotha floridana* (Fig. 3, A to E), both of which are pollinators of thermogenic cycads (*15*, *25*, *26*). In both species, we found that the most distal antennal segment was enriched in sensilla that were morphologically consistent with a thermosensitive function (Fig. 3, A to F, and fig. S5, A to G).

We first used single-sensillum electrophysiology to confirm that sensilla at the antennal tip of the beetle pollinator *P. floridana* were indeed thermosensitive. Heat elicited responses from two morphologically distinct coeloconic sensilla: the first housed a neuron that responded instantly to increased temperature (Fig. 3, G and H), and the second consisted of two classes of neurons that were activated and inhibited by heat (Fig. 3, G and H, and fig. S5, J and K). By contrast, hair-like mechanosensory sensilla responded to touch but not temperature (Fig. 3, G and H). To investigate whether these thermosensitive structures are important for thermal IR sensation, we measured

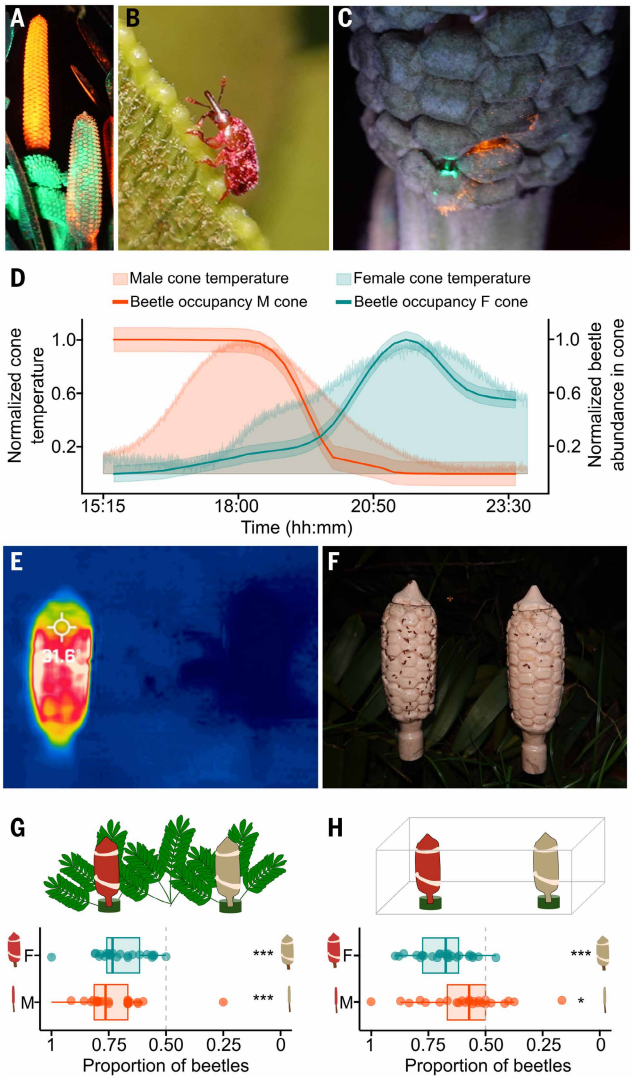

Fig. 2. Thermal IR is a pollination signal for specialized beetle pollinators. (**A**) Male cones of the cycad *Z. furfuracea* releasing pollen marked with UV-fluorescent dyes to track beetle movement. (**B**) A beetle pollinator (*R. furfuracea*) covered in pollen and UV-fluorescent dyes while carrying pollen from male to female plants. (**C**) Female cone of *Z. furfuracea* showing marks of fluorescent dyes left by beetle pollinators during pollen transfer. (**D**) Beetle occupancy of male and female cones during thermogenesis. n = 570 beetles in male cones; n = 278 beetles in female cones. (**E**) Field experiments using heated (left) and nonheated (right) 3D-printed models of female cones. (**F**) Beetle pollinator visits to artificially heated 3D-printed cones (left) versus those at ambient temperature (right). (**G**) Proportion of beetles visiting heated (left) and nonheated (right) 3D-printed models of male and female cones in field experiments. Female cones: n = 25 experiments, n = 1025 beetles, $P < 0.0001$. Male cones: n = 31 experiments, n = 518 beetles, $P < 0.0001$. (**H**) Proportion of beetles visiting heated (left) and nonheated (right) 3D-printed models of male and female cones in cage experiments controlling for conductive and convective heat. Female cones: n = 26 experiments, n = 1187 beetles, $P < 0.0001$. Male cones: n= 25 experiments, n = 1154 beetles, $P < 0.001$. Boxplots represent the interquartile range, and midlines represent the median.

the behavioral responses of immobilized beetles to thermal IR and used a cone odorant (methyl salicylate) as a positive control (Fig. 3I and figs. S5L and S6). Beetles responded to both cues, but only thermal IR responses were abolished by microdissection of the thermosensitive antenna tip (Fig. 3, I and J). These results suggest that beetles detect IR using specialized sensilla at the tips of their antennae.

TRPA1 underlies IR sensing in beetles

To determine the molecular basis of IR sensation, we first performed transcriptome analysis in beetle antennae and other reference organs from *P. floridana*. Transcripts from candidate thermosensitive genes were enriched in the antennae, including *GR28b* (Gustatory Receptor 28b), *IR21a* (Ionotropic Receptor 21a), and several splice variants of *TRPA1* (Transient Receptor Potential Ankyrin 1) (Fig. 4A). In situ hybridization showed that beetle *TRPA1* was restricted to distinct sensory neurons in the most distal antennal segment, which is required for IR sensation (Fig. 4, B and C). *GR28b* and *IR21a*, which detect heating (*27*) and cooling (*28*), respectively, were not coexpressed with *TRPA1* (fig. S7, A to D). Instead, *GR28b* and *IR21a* colocalized within different sensilla, consistent with functional measurements demonstrating two neurons with contrasting responses to temperature (figs. S5K and S7, A to D). Opsins can colocalize with *TRPA1* to facilitate thermal IR sensation in mosquitoes (*29*), but we did not detect opsin expression in the beetle antenna (fig. S9A).

TRPA1 contributes to IR perception in snakes and mosquitoes (*29*, *30*), suggesting that it has a convergent role as a thermal IR sensor across diverse taxa. Because transcripts for a short isoform (B) of *TRPA1* were the most highly expressed in the beetle antenna, we further investigated its putative function as a thermoreceptor using patch-clamp electrophysiology (Fig. 4D). Heterologous expression of *P. floridana TRPA1*(B) exhibited robust responses to temperatures even just slightly above ambient (Fig. 4D and fig. S7). To determine whether *TRPA1*(B) contributes to beetle IR sensation, we exploited the observation that *TRPA1*(B) has ancestral electrophile sensitivity and screened 30 putative antagonists of *TRPA1*(B) using calcium imaging. Whereas common antagonists of vertebrate, fly, and mosquito *TRPA1* failed to block beetle *TRPA1*, we identified AM-0902 as a potent blocker of beetle *TRPA1* (fig. S7, F to I). Ectopic application of AM-0902 to the beetle antennae abolished behavioral responses to thermal IR, but did not affect responses to cone odorants (Fig. 4E and fig. S7E).

We reasoned that if beetle *TRPA1*(B) is specialized for IR sensation, then it should exhibit structural adaptations that enhance thermal sensitivity. To determine the structural basis of heat sensitivity in beetle *TRPA1*(B), we leveraged comparative analysis with *TRPA1*(A), the second most highly expressed isoform in beetle antennae (Fig. 4A). Sequence analysis and AlphaFold (*31*) modeling revealed that the isoforms only differed in a relatively small region, with *TRPA1*(B) having a shorter N terminus (Fig. 4F). Despite exhibiting only this subtle difference, *TRPA1*(B) had significantly greater thermosensitivity compared with *TRPA1*(A) ($P < 0.0001$; Fig. 4G). *R. furfuraceae*, a distantly related beetle species that is also a pollinator of thermogenic cycads, also had *TRPA1*(B) that exhibited enhanced thermosensitivity relative to its *TRPA1*(A) (Fig. 4G). Isoform-specific differences in *TRPA1* thermosensitivity are also present in fruit flies and mosquitoes (*32*), and our findings in beetles suggest that *TRPA1* splicing evolved at least 300 Ma. Additionally, selection analyses of insect *TRPA1*(B) revealed that the N terminus is a hotspot for adaptive evolution (Fig. 4H). Even among beetle pollinators of thermogenic plants, the N terminus exhibited the highest divergence, highlighting its potential role as a modulatory region controlling thermosensitivity properties.

If *TRPA1*(B) is involved in sensing plant species–specific IR signals for pollination, then we hypothesized that species-specific activation ranges would reflect temperature profiles reached by their respective thermogenic host plants. Indeed, *P. floridana TRPA1*(B) exhibited robust heat-evoked activity to temperatures in the thermal range of its thermogenic host plant (*Zamia integrifolia*; Fig. 4, I and J). Similarly, *TRPA1*(B) from the beetle *R. furfuraceae* exhibited a distinct thermal activation range that was differentially tuned to its specific host plant (*Z. furfuracea*) temperature range during thermogenesis (Fig. 4, I and J). These beetle pollinators, from families separated by >140 Ma (*33*), are both attracted to IR signals, suggesting that IR detection may be a widespread

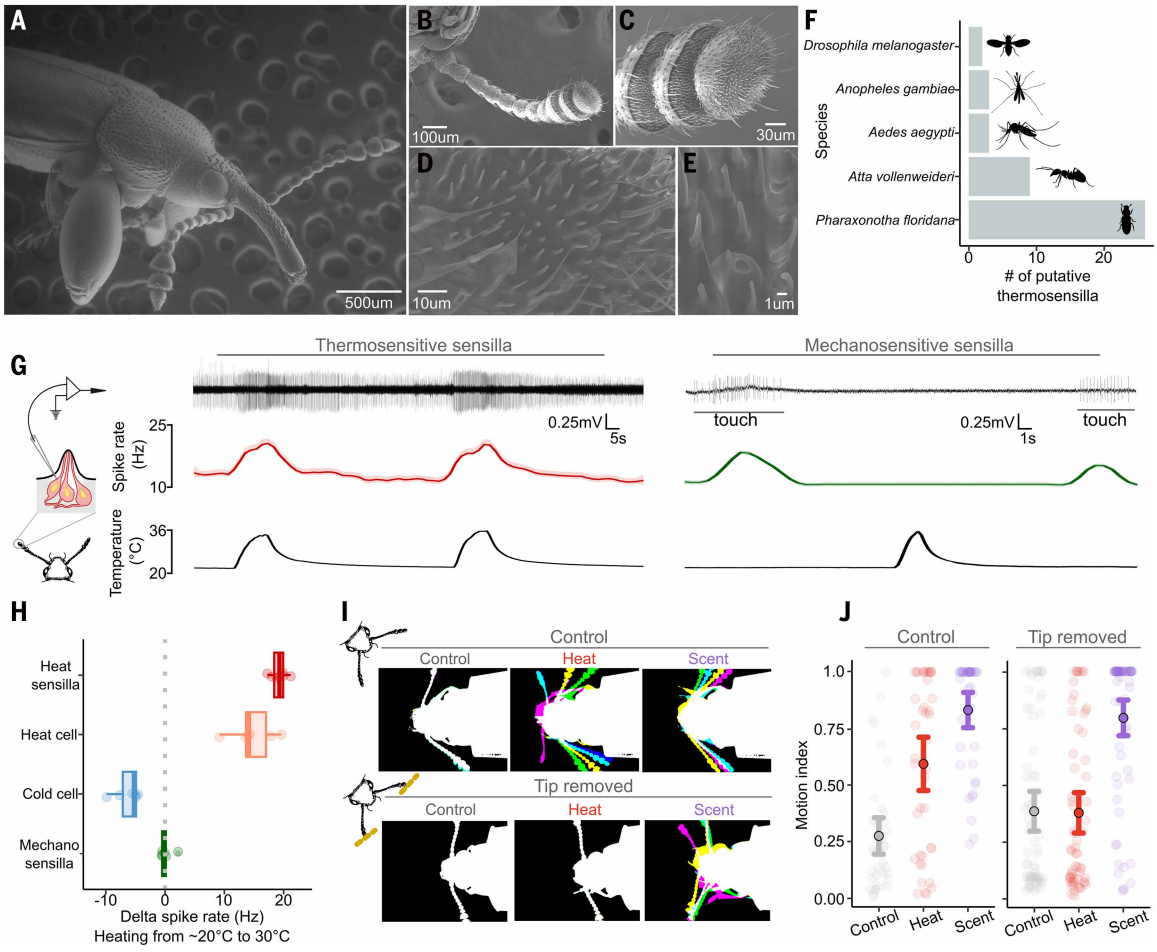

Fig. 3. Pollinators of thermogenic plants have specialized organs at the tip of their antennae to sense thermal radiation. (**A**) Scanning electron micrograph (SEM) images of the beetle pollinator *R. furfuracea*, which pollinates the thermogenic plant *Z. furfuracea*. (**B**) SEM image of an antenna from the beetle pollinator *P. floridana*, which pollinates the thermogenic plant *Z. integrifolia.* (**C**) SEM image of the last three antennal segments of *P. floridana* showing the sensory organs (sensilla). (**D**) Magnified view of sensilla diversity in the terminal antennal segment of *P. floridana*. (**E**) SEM image showing the morphology of a thermosensitive coeloconic peg-in-pit sensillum in the terminal antennal segment of *P. floridana*. (**F**) Number of thermosensitive sensilla ("thermosensilla") in different insect species. (**G**) Left, neuronal responses to heat radiation from a single thermosensitive sensillum located in the terminal antennal segment of the beetle *P. floridana*. Right, neuronal responses to heat radiation and touch from a mechanosensitive sensillum in the terminal antennal segment. (**H**) Changes in firing rate from different antennal sensilla in response to heating from ~20° to ~30°C ($P < 0.0001$ for thermosensitive sensilla responses to heat, $n = 6$ to 7 sensilla; boxplots represent interquartile range, and midlines represent median). (**I** and **J**) Antennal movements of beetle pollinators with (control) and without the last antennal segment (tip removed) in response to heat radiation and cone scent. Colors represent different time frames indicating antennae movement. $n = 40$ to 67 beetles. Error bars represent the 95% confidence interval, and midpoints represent the mean.

strategy among pollinators of thermogenic plants. Thus, our data suggest that *TRPA1*(B) might play an important role in IR sensation and mutualistic plant-pollinator signaling, in contrast to IR detection being previously associated with predation or parasitism (*29*, *30*).

IR signaling predates flower colors

Flowers and cones serve as "billboards" using multiple signals to lure pollinators (*1*). These signals can be effective hierarchically at different spatial and temporal scales (*1*). Floral scent, a long-range signal widely used across seed plants (fig. S8), can attract pollinators over meters (*3*). However, scent becomes uninformative at close range without additional short-range cues such as colors that guide pollinators to nectar (*1*, *3*). We discovered that IR is effective at short- and midrange distances, advertising cones that release and receive pollen. Given the dominance of color as a cue in these ranges, we investigated, in a comparative framework, whether it complements or is redundant to thermal IR by mapping both signals across seed plants.

If ancient plant-pollinator interactions rely on metabolic signals rather than color, then flower and cone colors would probably exhibit lower chromatic contrast under vision models of early pollinators. To investigate beetle color vision, we mined opsins from our transcriptome dataset, identifying a UV and a long-wavelength (LW) opsin (figs. S9 and S10A). Using heterologous expression and spectrophotometry, we found that the UV and LW opsins showed maximum absorbance spectra (λ_{max}) at ~374 nm (UV) and ~490 nm (green) (Fig. 5, A and B). This dichromatic visual system in cycad pollinators is consistent with beetles having lost the short-wavelength opsin from a trichromatic insect ancestor (*34*) (fig. S9).

We next evaluated whether cones and flowers present salient visual signals to key pollinators, including beetles, bees, and butterflies. We recorded reflectance spectra of cones from 23 cycad species (Fig. 5C and fig. S10C) and gathered reflectance spectra data across 1000 species of flowering plants from the FReD database (*35*) (fig. S10B). We mapped both cone and flower reflectance spectra into the respective color space models of the different pollinators (Fig. 5, D to F). Cone spectra did not overlap with beetle opsin sensitivities, suggesting poor discrimination under beetle vision (Fig. 5C). By contrast, flowers exhibited higher chromatic contrast under the visual model of more

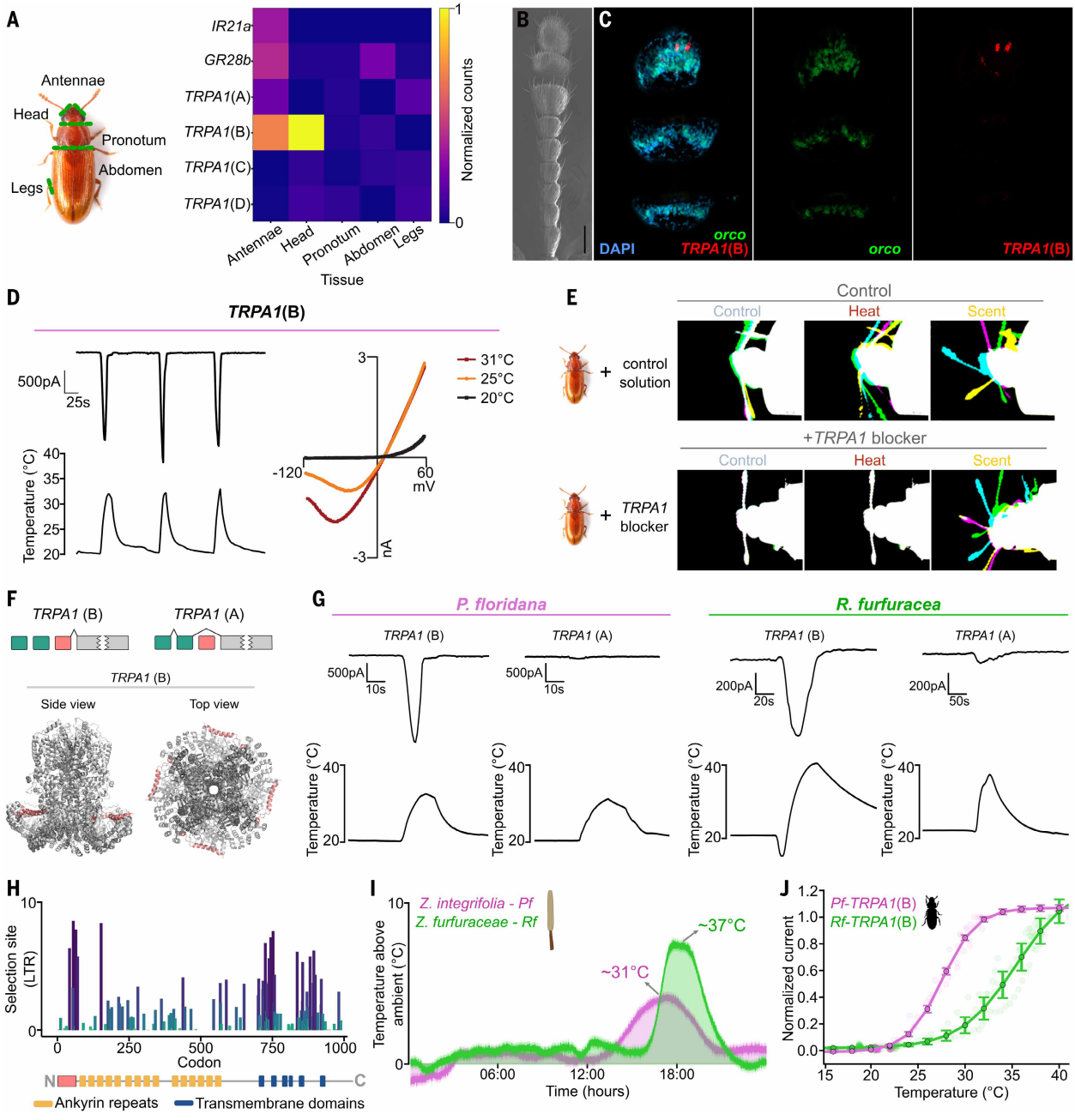

Fig. 4. Molecular basis of IR sensing in pollinators of thermogenic plants. (**A**) Left, beetle tissue samples used for comparative transcriptomics. Right, expression of candidate thermosensitive genes in different organs of the beetle pollinator *P. floridana*. (**B**) SEM image of a beetle antennae. Scale bar, 100 μm. (**C**) In situ hybridization of the last three antennal segments of the beetle pollinator *P. floridana* showing the expression of the candidate thermosensitive gene *TRPA1*(B) and the olfactory sensory neuron marker *orco*. (**D**) Temperature-dependent currents of heterologously expressed *TRPA1*(B). $n = 9$ cells, $P < 0.0001$. (**E**) Antennal movement of beetle pollinators to heat radiation and cone scent for beetles untreated and treated with the *TRPA1* antagonist AM-0902. $n = 32$ beetles, $P < 0.0001$. (**F**) *TRPA1*(B) and *TRPA1*(A) splice isoforms. Colored blocks represent exons that are alternatively spliced (top). AlphaFold structure highlights in color the position of the amino acids encoded by the exon, which is unique to the *TRPA1*(B) variant. (**G**) Temperature-dependent currents of *TRPA1*(B) and *TRPA1*(A) compared across two beetle pollinators (*P. floridana* and *R. furfuracea*). $n = 6$ to 9 cells, $P < 0.0001$. (**H**) Selection analysis of *TRPA1*(B) across >50 species from different insect orders. (**I**) Thermogenic profiles of plants pollinated by *P. floridana* (*Z. integrifolia*, lower temperature, pink) and *R. furfuracea* (*Z. furfuracea*, higher temperature, green). Data are representative of $n = 4$ to 25 plants. (**J**) Heat responses of *TRPA1*(B) channels from *P. floridana* (pollinates lower-temperature cones, pink) and *R. furfuracea* (pollinates higher-temperature cones). $n = 3$ to 9 cells. Error bars represent standard error of the mean.

recent pollinators such as bees and butterflies (Fig. 5, E and F, and fig. S10D). These findings support a shift from ancient metabolic signaling to the diversification and stunning elaboration of color signals characteristic of flowering plants today (Fig. 5H).

To test this pattern, we mapped thermogenesis and color diversity across major families of seed plants. We surveyed the literature (*35*–*38*) and the TRY Plant Trait Database (*39*) and developed an AI pipeline to extract large-scale color data from community-science platforms. We found that thermogenesis has evolved independently in cycads and angiosperms and is disproportionately represented in early-diverging lineages of seed plants (Fig. 5, G and H, and fig. S12), consistent with the fossil evidence (*40*). By contrast, more recently diversified lineages,

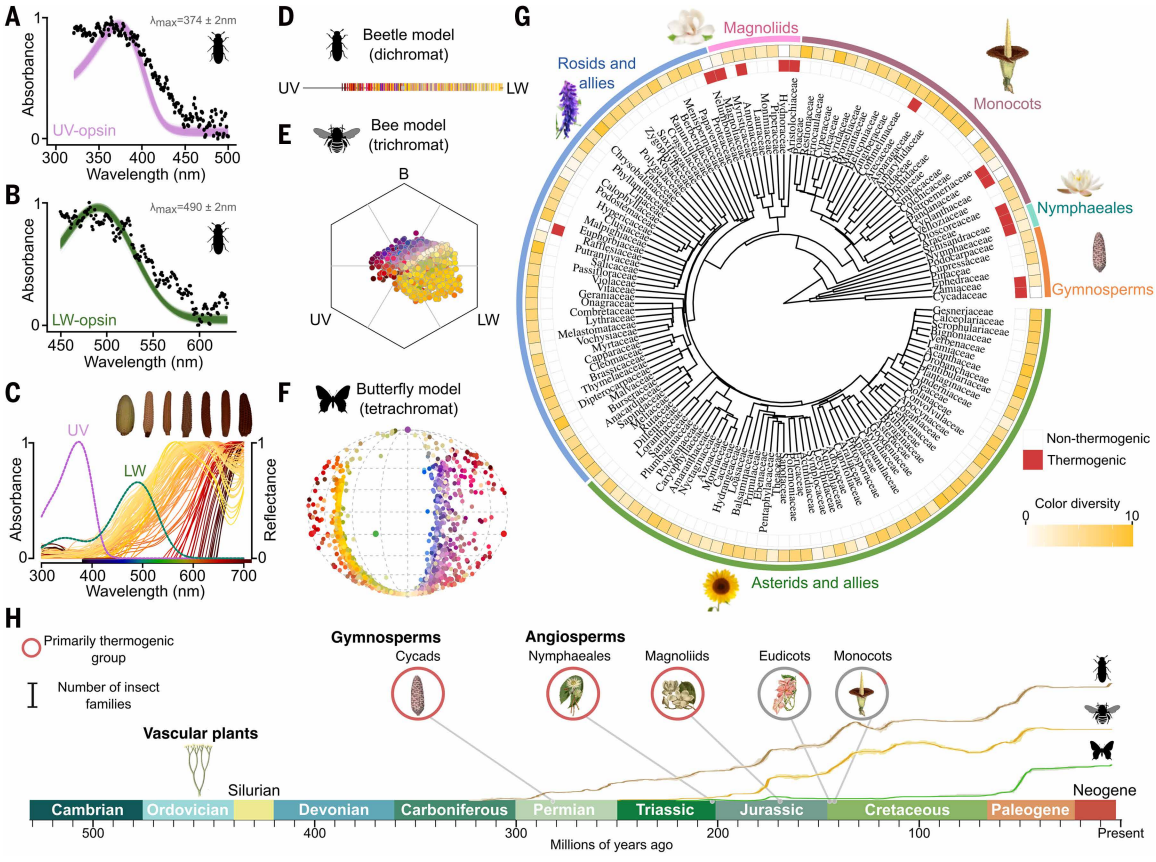

Fig. 5. Thermogenesis is an ancient pollination signal exhibiting a trade-off with color diversity. (**A** and **B**) Absorbance spectra of the two purified beetle opsins, UV and LW. (**C**) Absorbance spectra of the two beetle visual opsins UV and LW with the reflectance spectra of cycad cones pollinated by beetles ($n = 115$ cones, $n = 5$ samples across 23 species). The cones above the plot are representative of the color variation across species. (**D** to **F**) Reflectance spectra of >1000 species of cycads and flowering plants as modeled with the dichromatic visual system of a cycad beetle pollinator (D), the trichromatic visual system of a bee pollinator (E), and the tetrachromatic visual system of a butterfly pollinator (F). Each point represents a cone or flower color projected into the pollinator's perceptual space. Distances between points indicate perceptual contrast; the farther apart, the more distinguishable the colors appear to that visual system. For reference, points are colored using human vision approximations of the color produced by the spectra. (**G**) Thermogenesis and color diversity mapped as traits onto the phylogeny of seed plants (Spermatophyta). (**H**) Timeline of major plant clade evolution and accumulated diversification of insect families through geological time for three large pollinator insect orders: Coleoptera (beetles), Hymenoptera (bees, wasps, and ants), and Lepidoptera (moths and butterflies). Bayesian diversification rates are as estimated in (*41*) using the family-level fossil dataset from (*42*). The scale bar for the number of insect families represents 25 lineages.

such as the rosids and asterids, exhibit diverse colors and are characterized by metabolic investments in a broad range of floral pigments (Fig. 5G). Maximum likelihood models revealed a negative correlation between thermogenesis and color diversity ($P = 1.14 \times 10^{-9}$; figs. S10E and S11 and table S6), indicating an evolutionary trade-off whereby seed plant families that exhibit thermogenesis show low color diversity and vice versa. This negative trade-off is likely mediated by functional redundancy of pollination signals, different metabolic costs associated with heat and color pigment production, and the exploitation of sensory biases of diverse primary pollinator groups.

To further explore the shift from IR- to color-based pollination, we estimated the origin of thermogenesis and gathered fossil data on thermogenic plants and insect pollinators. Because cycads are the oldest living plants pollinated by animals, we first performed ancestral state reconstruction of thermogenesis in this group to pinpoint the evolution of this pollination strategy (fig. S13). We then surveyed family-level fossil records of thermogenic plants (*40*) (table S7) and recent Bayesian estimates of diversification rates for major pollinator insect orders (*41*, *42*) (Fig. 5H and table S8). Collectively, these data support that: (i) thermogenesis evolved at the base of Cycadales in the early Permian (~275 Ma) and represents one of the most ancient pollination syndromes (figs. S12 and S13 and tables S7 and S8); (ii) beetles were ancestrally nocturnal, dichromatic, and among the earliest pollinators of seed plants (*17*, *40*, *43*) (Fig. 5H, figs. S9 and S14, and table S8); and (iii) beetle diversification predated the rise of polychromatic pollinator lineages such as bees and butterflies, which evolved largely concurrently with the adaptive radiation of modern flowering plants, particularly after 50 Ma (*41*, *42*) (Fig. 5H, fig. S9, and table S8). These findings point to an evolutionary shift in pollination signaling strategies that coincided with changes in dominant pollinator groups, each characterized by distinct sensory biases.

Discussion

The evolution of pollination reflects the interplay between plant signals and pollinator sensory abilities. Early pollinator interactions likely recruited ancient molecular machinery already present in plant metabolism and pollinators' senses. Here, we found that the molecular bases of thermogenesis and IR sensing involve the ancient proteins AOX1 and TRPA1, respectively. Although widespread in plants (*44*) and animals (*45*), the up-regulation of these proteins supports specialized adaptations for heat production and detection. The regulatory nature of these adaptations likely contributed to their evolution, with

AOX1-driven thermogenesis emerging independently in nonflowering and flowering plants (*13, 19, 20*) and TRPA1-mediated IR sensation evolving in distantly related beetle pollinators, mosquitoes (*29*), and snakes (*30*). Thus, thermogenesis and IR sensing represent remarkable cases of convergence, where selection repeatedly coopted the same molecular toolkit to enhance thermal signaling and perception across diverse lineages.

Once sensory biases for metabolic cues such as heat evolved in gymnosperm pollinators, early pollinators may have exploited similar cues in nascent groups of flowering plants. Although cycads are currently the most threatened plant order (*46*), they were considerably more diverse and ecologically dominant during the Mesozoic (*47*), coexisting with early-diverging lineages of angiosperms. Fossil evidence from the mid-Cretaceous supports host plant shifts of cycad beetle pollinators to basal angiosperm lineages such as water lilies (Nymphaeaceae) (*43*), which, like cycads, are thermogenic. This early establishment of thermogenesis and IR signaling between gymnosperms and beetles likely set the stage for efficient, insect-mediated pollination at the onset of flowering plants.

Although the earliest flowers were mostly thermogenic and visually inconspicuous (*40*, *48*), color-based syndromes now dominate modern ecosystems. This transition in signaling did not coincide with the origin of flowers (*41*). Instead, this shift occurred alongside the expansion of major groups of diurnal pollinators such as bees and butterflies (*41*), which have retained and elaborated trichromacy. Beetle pollinators of thermogenic plants are dichromatic, yet recent radiations of beetle groups that visit flowers show opsin duplications with putative tri- and tetrachromatic visual systems but only in diurnal species (*49*). These large-scale patterns underscore how pollinator sensory systems are primary drivers shaping the evolution of floral traits. Indeed, as different plant lineages rose to ecological dominance, their signals evolved to tap into the preexisting sensory biases of the widespread pollinator groups. More broadly, our results suggest that metabolic cues such as IR played a pivotal role in the early evolution of biotic pollination, one of the most transformative mutualisms for ecosystems in Earth's history.

REFERENCES AND NOTES

1. R. A. Raguso, *Curr. Opin. Plant Biol.* **7**, 434–440 (2004).
2. S. Salzman *et al.*, *Curr. Biol.* 0 (2023).
3. A. Dahake *et al.*, *Nat. Commun.* **13**, 7773 (2022).
4. R. S. Seymour, P. Schultze-Motel, *Endeavour* **21**, 125–129 (1997).
5. L. B. Thien, H. Azuma, S. Kawano, *Int. J. Plant Sci.* **161** (S6), S225–S235 (2000).
6. C. Lance, *Plant Sci. Lett.* **2**, 165–171 (1974).
7. R. M. Knutson, *Science* **186**, 746–747 (1974).
8. B. J. D. Meeuse, I. Raskin, *Sex. Plant Reprod.* **1**, 3–15 (1988).
9. R. S. Seymour, C. R. White, M. Gibernau, *Nature* **426**, 243–244 (2003).
10. M. J. Harrap, S. A. Rands, N. Hempel de Ibarra, H. M. Whitney, *eLife* **6**, e31262 (2017).
11. R. M. Borges, H. Somanathan, A. Kelber, *Q. Rev. Biol.* **91**, 389–418 (2016).
12. S. Salzman, D. Crook, J. D. Crall, R. Hopkins, N. E. Pierce, *Sci. Adv.* **6**, eaay6169 (2020).
13. Y. Ito-Inaba *et al.*, *Plant Physiol.* **180**, 743–756 (2019).
14. W. A. Valencia-Montoya, D. Tuberquia, P. A. Guzmán, J. Cardona-Duque, *Arthropod-Plant Interact.* **11**, 717–729 (2017).
15. W. Tang, *Bot. Gaz.* **148**, 165–174 (1987).
16. H. Qian, J. Zhang, *J. Syst. Evol.* **52**, 423–430 (2014).
17. C. Cai *et al.*, *Curr. Biol.* **28**, 2806–2812.e1 (2018).
18. C. Claudel, O. Loiseau, D. Silvestro, S. Lev-Yadun, A. Antonelli, *Plant J.* **115**, 874–894 (2023).
19. A. Zulfiqar *et al.*, *PNAS Nexus* **3**, pgae492 (2024).
20. R. Li, J. Li, S. Wang, R. Wang, *Int. J. Mol. Sci.* **23**, 11950 (2022).
21. C. L. Hughes, Y. An, J. N. Maloof, S. L. Harmer, *Plant Direct* **8**, e573 (2024).
22. I. Terry, G. H. Walter, C. Moore, R. Roemer, C. Hull, *Science* **318**, 70–70 (2007).
23. E. Hallberg, B. S. Hansson, *Microsc. Res. Tech.* **47**, 428–439 (1999).
24. M. Nagel, C. J. Kleineidam, *Front. Behav. Neurosci.* **9**, 240 (2015).
25. K. J. Norstog, D. Wm. Stevenson, K. J. Niklas, *Biotropica* **18**, 300–306 (1986).
26. W. Tang, *Am. J. Bot.* **74**, 90–99 (1987).
27. L. Ni *et al.*, *Nature* **500**, 580–584 (2013).
28. C. Greppi *et al.*, *Science* **367**, 681–684 (2020).
29. A. Chandel *et al.*, *Nature* **633**, 615–623 (2024).
30. E. O. Gracheva *et al.*, *Nature* **464**, 1006–1011 (2010).
31. J. Abramson *et al.*, *Nature* **630**, 493–500 (2024).
32. K. Kang *et al.*, *Nature* **481**, 76–80 (2011).
33. D. D. McKenna *et al.*, *Proc. Natl. Acad. Sci. U.S.A.* **116**, 24729–24737 (2019).
34. C. R. Sharkey *et al.*, *Sci. Rep.* **7**, 8 (2017).
35. S. E. J. Arnold, S. Faruq, V. Savolainen, P. W. McOwan, L. Chittka, *PLOS ONE* **5**, e14287 (2010).
36. M. Shrestha *et al.*, *Data Brief* **54**, 110512 (2024).
37. A. Gutiérrez *et al.*, *Sci. Data* **12**, 594 (2025).
38. E. Narbona *et al.*, *Sci. Rep.* **15**, 15927 (2025).
39. J. Kattge *et al.*, *Glob. Chang. Biol.* **26**, 119–188 (2020).
40. D. Peris *et al.*, *Nat. Plants* **10**, 1297–1303 (2024).
41. D. Peris, F. L. Condamine, *Nat. Commun.* **15**, 552 (2024).
42. F. L. Condamine, M. E. Clapham, G. J. Kergoat, *Sci. Rep.* **6**, 19208 (2016).
43. D. Peris *et al.*, *iScience* **23**, 100913 (2020).
44. R. J. Weaver, A. E. McDonald, *Biochim. Biophys. Acta Bioenerg.* **1864**, 149003 (2023).
45. W. A. Valencia-Montoya, N. E. Pierce, N. W. Bellono, *Annu. Rev. Cell Dev. Biol.* **40**, 353–379 (2024).
46. M. P. Griffith *et al.*, *Int. J. Plant Sci.* **176**, 1–10 (2015).
47. M. Coiro, L. J. Seyfullah, *Commun. Biol.* **7**, 328 (2024).
48. H. Sauquet *et al.*, *Nat. Commun.* **8**, 16047 (2017).
49. C. R. Sharkey, G. S. Powell, S. M. Bybee, *Front. Ecol. Evol.* **9**, 676369 (2021).

ACKNOWLEDGMENTS

We thank the Montgomery Botanical Center for providing infrastructure for fieldwork, sample collection, and behavioral experiments, with special thanks to P. Griffith, J. Tucker Lima, M. J. Sanín, X. Gratacos, D. Tucker, and V. Ramirez; the Carlson lab at Yale University, particularly H. Dweck and Y. Luo, and the Garrity lab at Brandeis University for support with single sensillum recordings; E. Soucy and Y. Li at the Harvard Center for Brain Science for help with scanning and printing cycad cones for behavioral experiments, advice on heat delivery systems, and assistance with spectrometer measurements of cycad cones; M. Ericsson and A. Nordstrom at the Harvard Medical School Electron Microscopy Facility for support with imaging; W. Tang and P. Skelley for providing beetle specimens for molecular and behavioral experiments; M. Tevelonis from Botanics Wholesale for generously donating potted cycads for field experiments; the Kampong National Tropical Botanical Garden, the Fairchild Botanical Garden, and the Medellín Botanical Garden (JAUM); B. de Bivort, B. Farrell, and S. Eddy for guidance; C. Allard, P. Villar del Rio, and J. Thibodeau for help with electrophysiology, RNAscope, and behavioral experiments; all members of the Pierce and Bellono labs and members of the Losick, Nett, and Elya labs for their valuable discussions on this work; and G. M. Montoya Giraldo and G. Valencia Ramos for support and encouragement throughout all stages of this project. **Funding:** This work was supported by a Lemann grant to N.E.P and R.C.; a Mind, Brain, and Behavior Interfaculty grant to N.E.P. and N.W.B.; a Harvard Museum of Comparative Zoology Putnam Expedition grant to W.A.V.-M.; a New York Stem Cell Foundation grant to N.W.B.; FRS-FNRS grant MISU F6002.24 to M.A.L.; National Institutes of Health grant R35GM142697 to N.W.B.; a Moore Foundation EPI grant 11561 to N.Y. and C.-C.T. a Harvard OEB and MCZ fellowship to W.A.V.-M.; a Fulbright-Colciencias Fellowship to W.A.V.-M.; and a Harvard Ashford Fellowship in the Natural Sciences to W.A.V.-M. **Author contributions:** Conceptualization: W.A.V.-M., N.E.P., N.W.B.; Formal analysis: W.A.V.-M.; Funding acquisition: N.E.P., R.C., M.A.L., W.A.V.-M., N.W.B.; Investigation: W.A.V.-M., M.A.L., N.R., M.C.; Methodology: W.A.V.-M., N.E.P., N.W.B.; Project administration: N.E.P., N.W.B.; Resources: W.A.V.-M., M.A.L., N.R., M.C., S.S., C.-C.T., N.Y., J.C., R.C., N.E.P., N.W.B.; Supervision: N.E.P., N.W.B.; Visualization: W.A.V.-M.; Writing – original draft: W.A.V.-M., N.W.B.; Writing – review & editing: W.A.V.-M., M.A.L., N.R., M.C., S.S., C.-C.T., N.Y., J.C., R.C., N.E.P, N.W.B. **Competing interests:** The authors declare no competing interests. **Data and materials availability:** All transcriptomic data are available through the Sequence Read Archive (SRA) repository under BioProject accession codes PRJNA1315209 (beetles) and PRJNA1315211 (cycads). *Z. furfuracea* sequences: SRR35626714-SRR35626720; *R. furfuracea* sequences: SRR35658691 to SRR35658697; *P. floridana* sequences: SRR35626828-SRR35626832. Other data are available in the main text, the supplementary materials, and the references therein.

SUPPLEMENTARY MATERIALS

science.org/doi/10.1126/science.adz1728
Materials and Methods; Figs. S1 to S14; Tables S1 to S8; References (*50–114*);
MDAR Reproducibility Checklist

Submitted 20 May 2025; accepted 8 October 2025

10.1126/science.adz1728